



# Experimental assessment on aseismic capacity of a perimeter diagrid concrete core structure: Shake table tests

Di Wu<sup>a</sup>, T.Y. Yang<sup>b</sup>, Yan Xiong<sup>c,\*</sup>, Solomon Tesfamariam<sup>d</sup>

<sup>a</sup> Key Laboratory of Earthquake Engineering and Applied Technique of Guangdong Province, Guangzhou University, Guangzhou 510405, China

<sup>b</sup> Department of Civil Engineering, University of British Columbia, Vancouver V6T1Z4, Canada

<sup>c</sup> State Key Laboratory of Subtropical Building Science, South China University of Technology, Guangzhou 510640, China

<sup>d</sup> School of Engineering, University of British Columbia, Kelowna V1V 1V7, Canada

## ARTICLE INFO

### Keywords:

Perimeter diagrid concrete core structure  
Shake table test  
Seismic behavior  
Aseismic capacity assessment  
High-rise building

## ABSTRACT

Perimeter diagrid concrete core (PDCC) is a structural system used for high-rise building applications. Quantifying their seismic safety is of interest to owners and decision makers due to the lack of the comprehensive understanding of the seismic performance of the high-rise PDCC structure. To systematically evaluate the seismic performance, a 36-story PDCC structure has been assessed using 1/20 scaled shake table tests. In addition, a detailed nonlinear finite element model (FEM) of the PDCC structure was built for comparison and analysis with the shaking table test. The damage to the perimeter diagrid bracings, the RC structural walls, the diagonal beam, under earthquake excitations have been assessed and discussed systematically based on the experimental and numerical results. The analysis result shows that the PDCC structure has a high performance under the earthquake load that can be used as an efficient seismic force-resisting system. Under the action of horizontal earthquakes, the axial force of the diagonal braces on the same floor varies greatly, and the axial force of the diagonal brace is related to the number of other diagonal braces on its axis. In terms of seismic damage to the perimeter diagonal braces, the most severe seismic damage is concentrated in the diagonal braces with higher axial forces, while the damage to other diagonal braces with smaller axial forces is less severe. And the seismic damage of diagonal bracing has a tendency to expand to other surrounding diagonal braces.

## 1. Introduction

Sustainable and resilient high-rise buildings can be achieved with consideration of efficient structural system [1]. Vertical members of perimeter diagrid concrete core (PDCC) structure (Fig. 1a), tube-in-tube structural system, are developed by combining reinforced concrete (RC) core wall (Fig. 1b) and perimeter diagrid frame (Fig. 1c). The PDCC structural system has been used in a number of high-rise buildings (Sun 2015) [2,3,4]: Hearst Tower (182 m) in the United States, the Guangzhou Tower (610 m), the Guangzhou West Tower (437 m), the CCTV Tower (159 m) in China, the Doha Tower (238 m) in Qatar, the Dorobanti Tower (200 m) in Romania, and the Lotte World Tower (555 m) in South Korea.

A number of studies are reported on the seismic design and detailing of PDCC structures (e.g., [5,6,7]). The PDCC has high lateral stiffness and strength [8]. If designed and detailed properly, such structures

usually meet or exceeds performance of seismic code provisions [9,10]. The seismic behavior is governed by the diagonal angles, spectral shape factors, and aspect ratio of the diagrid [11,10]. Several studies have reported the seismic performance of diagrid structures analytically (e.g. [9,12]). The analytical and numerical studies should be corroborated with experimental test to investigate the interaction between the RC core and the perimeter diagrid system, and corresponding damage progression.

This paper presents a shake table test and numerical studies on a 36-story PDCC structure located in Shenzhen, China (Fig. 2). A 1/20 scaled model has been constructed and tested on the shake table located in Guangzhou earthquake engineering lab. The seismic performance of the prototype building observed from the shake table test has been systematically documented and used for analytical model validation. Failure mechanism and seismic capacity of the PDCC structure system under design earthquake intensity was investigated. Subsequently, the

\* Corresponding author at: State Key Laboratory of Subtropical Building Science, South China University of Technology, Guangzhou 510640, China.

E-mail addresses: [wudiwdzoo@gmail.com](mailto:wudiwdzoo@gmail.com) (D. Wu), [yang@civil.ubc.ca](mailto:yang@civil.ubc.ca) (T.Y. Yang), [24530938@qq.com](mailto:24530938@qq.com), [xyan@scut.edu.cn](mailto:xyan@scut.edu.cn) (Y. Xiong), [Solomon.Tesfamariam@ubc.ca](mailto:Solomon.Tesfamariam@ubc.ca) (S. Tesfamariam).

experimental results were used to verify nonlinear dynamic finite element simulation of the PDCC structure. Finally, the earthquake damage and the failure mode of the whole building under different seismic hazard levels have been investigated using the finite element method (FEM) and experimental results.

## 2. Experimental design and program

### 2.1. Description of PDCC prototype structure

Elevation and plan views of the PDCC building located in Shenzhen, China, are shown in Fig. 2a and 2b, respectively. The building has an above ground height of 162 m and typical floor dimension of 45 m × 45 m. The slabs and the perimeter spandrel beam are offset inside the diagrid system (Fig. 2b). The embedded steel beam in each story transfers the tension forces from the corner diagonal to the RC core wall.

Fig. 3a and 3b show the diagrid elevation view from 1st to 17th and 18th-36th stories, respectively. Fig. 3c and 3d show a typical corner column and diagrid joints, respectively. The diagonal beams (Fig. 3c) provide out-of-plan support of the perimeter diagrid system from the concrete core to the corner column joints of the perimeter diagrid system. The floor system is connected to the diagonal bracing nodes by externally extended box beams with full fusion penetration welding. Fig. 3d shows the specific connection between the diagonal bracing and the box beam of the floor system. In order to have reliable joint between diagonal (or box beam) and the concrete core, an H300 × 300 × 30 embedded in core has been welded with the diagonal. Every story that has a diagrid node at the corner column has a fully trussed story diaphragm to provide two load paths for unbalanced forces at the nodes. The primary system consists of the diagonal girder forming a diaphragm truss between the core and the perimeter spandrel. A secondary system consists of a diaphragm truss system at the perimeter of the story that stabilizes the box sections that connect to the nodes. The trusses and the corner diagonal floor beam resolve the hoop tension forces at the corner diagrid joints.

The dead load (DL, 100% of the gravity self-weight), superimposed dead load (SDL) and live load (LL) have been considered in the evaluation of the seismic performance of the structure. In addition to the actual self-weight of the structural elements, typical uniform SDLs were considered according to the load code for the design of building structures [14]. The SDL of the fill inside the core at the office floor (100 mm) is 2.4 kN/m<sup>2</sup>, outside the core finishing at office floors (50 mm) is 1.2 kN/m<sup>2</sup>, and roofing membrane and terrace (150 mm fill plus the insulation) is 5.25 kN/m<sup>2</sup>. The uniformly distributed LLs of the core area at the office floor is 3.5 kN/m<sup>2</sup>, and that of the office area outside the core

and the roof area is 2.0 kN/m<sup>2</sup>.

The prototype structure has been designed following the 2010 Chinese code for seismic design of buildings (CCSDB) [15]. The design strength of tension, compression, flexure, and shear is determined based on the 2003 Chinese code for steel structure [16]. For design service duration of 50 years, the structural safety level of the building is 2. In addition, importance factor of the structure is 1.0. Typical diagonal bracings, wide-flange composite beams, wide-flange columns, and built-up shapes have the minimum yield strength of 345 MPa and the minimum ultimate tensile strength of 470 MPa. Tables 1 and 2 show a summary of the dimension of diagonal bracings and the corner columns, respectively.

The structural steel members were calculated according to the design code (NSPRC 2003) under design seismic conditions. The design internal forces of the typical corner columns and perimeter diagonal bracings are shown in Table 3.

Table 4 shows a summary of the parameters of the concrete structural wall. The location of structural walls Q1, Q2, Q3 and Q4 can be referred to Fig. 2b. A typical end detail of the RC structural wall is shown in Fig. 4. The thicknesses of typical walls of structural walls (T1) in Fig. 4 were as shown in Table 4. A typical reinforcement of 1% is used for all the reinforced concrete core walls.

### 2.2. Model design and construction

Shake table tests have been used to test and evaluate the seismic performance of complex high-rise structures. The theory of structural models under dynamic loading is mainly based on Buckingham's PI-theorem, which describes the process main parameters of the physical equations can be transformed into dimensionless groups [17,18,19]. For a physical relation containing  $n$  physical variables, if there are  $r$  number of primary variables, it is always possible to combine the  $n$  physical quantities into  $n-r$  number of dimensionless terms  $\Pi_1, \Pi_2, \dots, \Pi_{n-r}$  and thus the physical equation can be expressed as:

$$F(\Pi_1, \Pi_2, \dots, \Pi_{n-r}) = 0 \quad (1)$$

For the similarity design of the building structure, it is necessary to satisfy the dynamic equilibrium relationship, material properties and boundary conditions. However, it is difficult to satisfy all the above physical equations. Thus, multiple control variables related to dimension ( $l$ ), acceleration ( $a$ ), and elastic modulus ( $e$ ) are presented to ensure geometric, material, and dynamic similarities [20]. Therefore, the following 3 primary variables are involved:

$$l; a; e(r = 3) \quad (2)$$

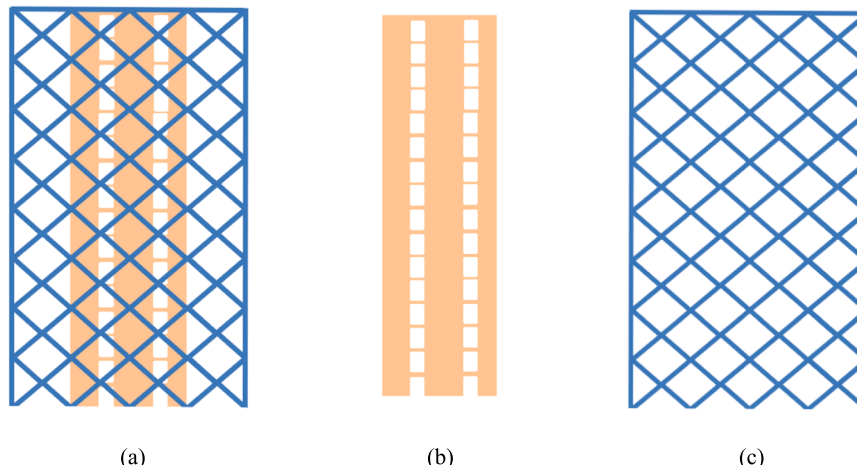


**Fig. 1.** (a) PDCC structure; (b) RC core wall; (c) perimeter diagrid braced mega frame.

The three primary variables can be expressed as functions of the three basic dimensional units (Force ( $F$ ), Length ( $L$ ), and Time ( $T$ )). Then, the Jacobian of these variables with respect to  $F$ ,  $L$ , and  $T$  are.

$$\frac{\partial(l, a, e)}{\partial(F, L, T)} = \begin{vmatrix} 0 & 1 & 0 \\ 0 & 1/(T)^2 & -2L/(T)^3 \\ 1/(L)^2 & -2F/(L)^3 & 0 \end{vmatrix} \neq 0 \quad (3)$$

The non-zero Jacobian indicates that dimensionally independent are independent. According to Buckingham's PI-theorem, for a typical structural dynamic model, the controlling condition can be expressed as (Harris and Habnisi 1999).

$$\Pi_1 = \sigma/e, \Pi_2 = \delta/l, \Pi_3 = f^2l/a, \Pi_4 = \rho la/e, \Pi_5 = q/(el^2), \Pi_6 = v \quad (4)$$

where  $\sigma$  is the dynamic stress,  $\delta$  is the deflection,  $f$  is the frequency,  $\rho$  is the mass density,  $q$  is the force, and  $v$  is Poisson's ratio. Here, the similarity relationship between the model and the prototype is mainly controlled by the above variables.

In determining the geometric similarity, the model needs to meet the dimensional constraints of the lab, i.e., the height of the model needs to be below the height limits of the lab and the base size of the model needs to be smaller than the size of the shake table. The different reported studies with different geometric similarity relationships are: 1/20 scaled model of the composite structure (Han et al. 2007), 1/20 scaled model of the wall structure with a transfer plate [22], and 1/15 scaled model of the multi-tower hybrid structure [23]. Owing to the restriction of the dimension of the shaking table, a 1/20 scaled prototype PDCC structure has been constructed and tested on the shake table.

When the geometric similarity ratio is small, the materials in the RC members of the model structure are in a low stress state, which can make it difficult to achieve similar relationships for the strength of the member sections. In order to satisfy the similar relationship between the sectional strength of the prototype and model structural members, the reinforcements of the RC members were designed according to the bending moment and shear force equivalence of the structural members. Steel members were designed in section using the similarity method of stiffness. Details of the derivation of the similarity relationship of the parameter variables in the model design are provided in the Appendix. Table 5 summarizes the scale factor of the shake table test.

Since the complex high-rise building consists of the micro-concrete, the galvanized iron wire and the shaped steel, the modulus-scale coef-

ficient of the entire model structure is difficult to be estimated accurately based on the material mechanical properties of several components. Therefore, it is necessary to estimate the similarity coefficient of the elastic modulus based on the experience of model fabrication after the model is completed. The modulus-scale coefficient of the experimental model was determined to be 1/3.5 based on the actual situation of a series of previously completed experimental models. This modulus-scale coefficient is consistent with the coefficient 1/3 to 1/5 for similar scaled building models using the same materials [20]. The acceleration similarity coefficient was determined to be 4 according to the loading capacity range of the shake table. As can be seen from Table 5, the main physical variables in the structural shaking test need to be satisfied:

$$S_m = S_e S_l^2 / S_a \quad (5)$$

$$S_f = (S_a / S_l)^{0.5} \quad (6)$$

The additional mass can be determined according to Eq. (5). The scale factor of the shaker test can be verified by testing the natural frequency of the model structure in the experiment. The main natural frequencies of the model structure were measured by shaking tests after adding additional masses to each story. If the error of the natural frequency of the model structure tested in the experiment exceeds the limit value, the modulus-scale coefficient of the model needs to be corrected according to Eqs. (5) and (6). To meet the scale factor requirements and the constructability, the test model is fabricated using a micro-concrete mix with the maximum size of aggregate not greater than 4 mm. Moreover, the rebar in the RC structural wall and the slab is replaced using the galvanized wire. The main properties for the galvanized iron wire are 16# with a cross-sectional area of 2.01 mm<sup>2</sup>, 18# with a cross-sectional area of 1.13 mm<sup>2</sup>, 20# with a cross-sectional area of 0.64 mm<sup>2</sup>, 22# with a cross-sectional area of 0.40 mm<sup>2</sup>. The average yield strength of the shaped steel and galvanized iron wire reaches up to 235 MPa.

The modulus of elasticity of micro-concrete is affected by the cement strength grade, water-cement ratio and sand ratio. The water-cement ratio and sand ratio had a significant effect on the modulus of elasticity of granular concrete, while the effect of cement strength grade was not significant. Therefore, in order to achieve a similar relationship for the modulus of elasticity, the water-cement ratio, sand ratio and cement strength grade need to be adjusted before each placement of granular

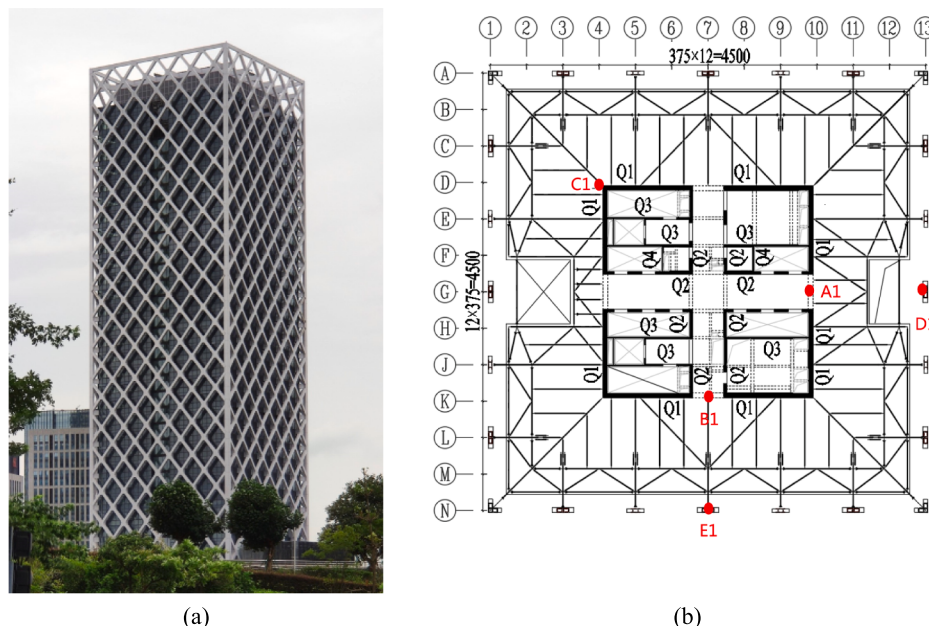


**Fig. 2.** (a) Overview of the PDCC structure; (b)Typical floor plan (Unit: cm; “●” denotes location of sensor).

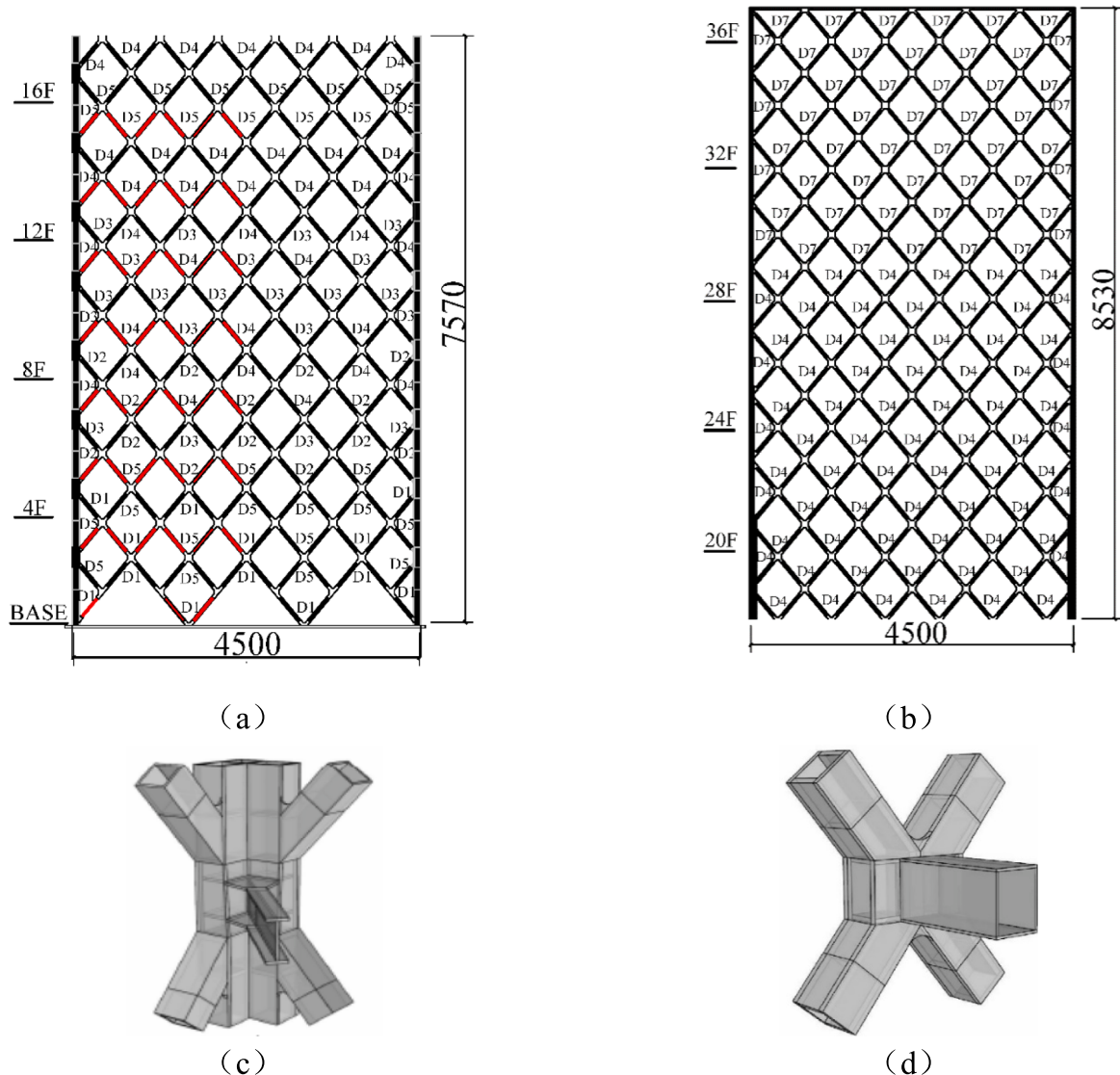


**Fig. 3.** Details of the diagrid bracing system of prototype (a) Elevation of perimeter steel diagrid bracings (1st – 18th story; red components denote locations of strain gauge); (b) Elevation of perimeter steel diagrid bracings (18th – 36th story); (c) 3D view of typical corner column joints; and (d) 3D view of typical diagrid joints (All length unit: cm).

**Table 1**  
Section dimension of perimeter diagonal bracings of prototype.

Number	Cross-section	$d_1$ (mm)	$d_2$ (mm)	$t_f$ (mm)	$t_w$ (mm)
D1		450	800	70	70
D2		450	700	70	70
D3		450	450	35	35
D4		450	450	30	30
D5		425	425	27	27
D7		350	425	25	20

**Table 2**  
Section dimension of corner column of prototype corner columns.

Story	Column section	$d_1$ (mm)	$d_2$ (mm)	$d_3$ (mm)	$t$ (mm)
22F-TOP		600	425	–	30
18F-21F		950	425	–	30
16F-17F		950	425	–	40
14F-15F		950	425	–	45
10F-13F		950	450	–	55
8F-9F		950	500	–	60
1F-5F		950	800	–	70
6F-7F		950	500	800	65

concrete, and cubic and prismatic specimens need to be prepared for mechanical property testing. In addition, experimental factors such as specimen size, shape, surface state, etc., will affect the test results of the micro-concrete strength. When the concrete specimen is compressed longitudinally along the loading direction, it will expand transversely.

**Table 3**

Typical internal forces of steel members under design earthquake conditions.

Position	Type	Compression Force (kN)	Major-axis bending moment (kN·m)	Minor-axis bending moment (kN·m)	Shear parallel with web (kN)
1F	Corner column	76278.13	1060.50	1284.63	416.75
	D4	17158.27	555.55	1097.34	48.50
	Corner column	44903.38	640.43	612.14	7.44
	D1	2937.58	149.32	51.69	28.43

**Table 4**

Parameters of RC structural wall of prototype.

Story	Cube compressive strength of concrete (MPa)	Wall thickness (mm)			
		Q1	Q2	Q3	Q4
14F-TOP	40	400	350	350	200
8F-14F	50	500	350	350	200
6F-8F	60	600	350	350	200
1F-6F	60	600	350	350	200

Since the transverse expansion of the loading plat is smaller than that of concrete, the friction force exists between the loading board and the concrete specimen, which restricts the transverse expansion of specimens. Thus, the standard for inspection and evaluation of concrete strength given by ACI [24] and NSPRC [25] specify the test standard specimens and test methods of concrete. Due to the size effect of the micro-concrete, the cube (70.7 mm × 70.7 mm × 70.7 mm) and the prism (70.7 mm × 70.7 mm × 230 mm) are adopted for the concrete compression strength and elastic modulus tests. The concrete's mechanical properties are determined based on the static experimental tests. According to the size of the specimen, the transfer coefficient of the standard cubic compressive strength is 0.95. The mechanical properties of the micro-concrete for each story are summarized in Table 6. Table 6 shows the micro-concrete types selected for different stories as M6, M8, M10 and M12, which corresponded to the micro-concrete mix ratios of cement, sand and water of 1:6.1:1.2, 1:5.6:1.1, 1:5:1, 1:4:7:0.9.

The dimensions of the steel members in the model are scaled down according to the similarity theory. In order to take this into account, the stresses in the model need to be similar when the material properties of the prototype and the model do not change. Thus, the principle of stiffness equivalence has been used in the cross-sectional design of the steel members [21,20]. The thicknesses and mechanical properties of the scaled perimeter diagrid frame are:

- Thickness of steel square tubes: 35 × 20 × 1.2 mm (D1), 35 × 20 × 1.2 mm (D2), 18 × 18 × 1.0 mm (D3), 18 × 18 × 0.8 mm (D4), 18 × 18 × 0.6 mm (D5).

- Thickness of I-shape steel beams: 15 × 12 × 1.0 × 1.0 mm (D7).
- Yield strength, ultimate strength, Young's modulus, and elongation of steel: 280 MPa, 370 MPa, 2.0 × 10<sup>5</sup> MPa, 25%.

A load combination of 1.0 DL + 1.0 SDL + 0.5 LL has been applied to the model according to 2010 CCSDB (NSPRC 2010a). To account for the LL and differences in material mass, additional masses have been added at each story using mass blocks. Additional masses were fixed to the floor slab of each floor using lead blocks with a mass of 10 kg each by resin glue. The lead blocks were carried to each floor by a lift and arranged by manually. The simulated earthquake tests have been conducted using the shake table test system (with the platform dimensions of 3 m × 3 m) with three dimensional and six degrees of freedom supplied by MTS Company. The vertical load-bearing capacity of the test system is 20 T with a maximum acceleration of 1.0 g in the two horizontal directions and 2.0 g in the vertical direction. The main property parameters of the shake table are shown in Table 7. The structure model during construction and the test model setup on the shake table is shown in Fig. 5.

### 2.3. Instrumentation and modal parameters

The acceleration and displacement were measured using a charge accelerometer (4381 V) with a charge amplifier (NEXUS 2692-014) from

**Table 5**

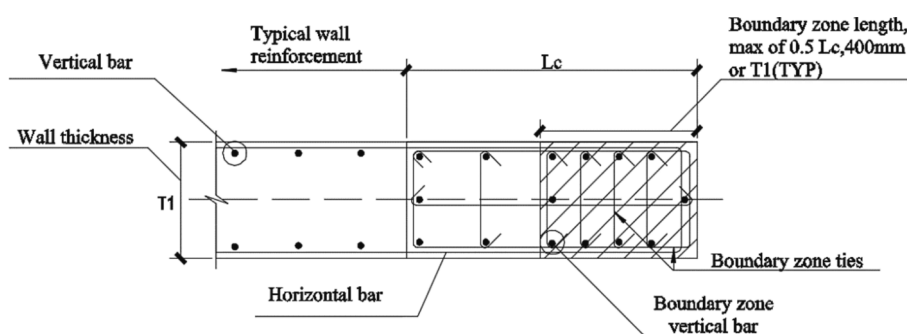
Scale factor of shaking table test.

Category	Symbol	Relationship	Similarity coefficient
Geometry-scale	$S_l$	$S_l$	0.05
Acceleration-scale	$S_a$	$S_a$	4
Elastic modulus-scale	$S_e$	$S_e$	0.29
Time-scale	$S_t$	$(S_l/S_a)^{0.5}$	0.11
Density-scale	$S_\rho$	$S_e/(S_l S_a)$	1.43
Mass-scale	$S_m$	$S_e S_l^2 / S_a$	$1.79 \times 10^{-4}$
Force-scale	$S_q$	$S_e S_l^2$	$7.14 \times 10^{-4}$
Frequency-scale	$S_f$	$(S_a/S_l)^{0.5}$	8.94
Strain-scale	$S_\epsilon$	1	1
Stress-scale	$S_\sigma$	$S_e$	0.29
Deflection-scale	$S_\delta$	$S_l$	1/20

**Table 6**

Mechanical Parameters of model micro-concrete.

Position	Type	Cube compressive strength(MPa)	Splitting tensile strength(MPa)	Young's modulus(MPa)
Floor slab	M6	6.25	0.87	12,053
26th-Top	M8	11.79	1.17	10,404
9th-25th	M10	10.16	1.29	11,704
1st-8th	M12	17.38	1.99	13,062

**Fig. 4.** Typical end detail of prototype RC structural wall.

**Table 7**  
Main parameters of shaking table test.

Main parameters	Direction	Parameter value (No load)	Parameter value (Full load)
Maximum acceleration (g)	X	$\pm 2.5$	$\pm 1.0$
	Y	$\pm 2.5$	$\pm 1.0$
	Z	$\pm 5.0$	$\pm 2.0$
Maximum velocity (mm/s)	X	$\pm 1000$	$\pm 800$
	Y	$\pm 1000$	$\pm 800$
	Z	$\pm 1000$	$\pm 500$
Maximum displacement (mm)	X	$\pm 100$	$\pm 100$
	Y	$\pm 100$	$\pm 100$
	Z	$\pm 50$	$\pm 50$

B&K, Denmark. A strain gauge (SPIDER8) from HBM, Germany, was used to collect the strain and its accompanying software (Catman) was used to collect the data. The converters of the Spider8 can operate synchronously for each channel with a 16-bit indexing per channel and a maximum rate of 9600 measurements/second. Each sensor is accurately calibrated for consistency on the shaking table prior to testing.

Twenty voltage-based displacement meters and twenty-eight voltage-based accelerometers have been used to measure the floor

accelerations and drifts. The specimen preparation and testing details are provided below. Table 8 presents the type and numbering of sensors for the test model. The acceleration and displacement sensors are placed every five stories and the locations are shown in Fig. 2b. The strains of concrete and the reinforcing steel bar of the RC core walls in the 1st story are monitored using the strain gauges (SPIDER8). To study the axial force distribution of the perimeter diagrid, a part of components in the whole perimeter diagrid have been placed, which can be seen in Fig. 3a. The strain gage sensitive grid size is  $3 \times 2$  mm, and the measured members are observed locally after each test to avoid the strain measurement being affected by local buckling. Owing to the restriction of the quantity of the strain gauges, a total of 45 diagonal bracings are installed.

After the test loading cases of each hazard class, the modal parameters of the model structure are measured, which can help to obtain the basic dynamic properties of the model structure. A Gaussian white noise excitation with the acceleration peak value of 0.05 g and the frequency bandwidth of 0.1 to 40 Hz has been adopted in the shake table tests for the modal parameter analysis. According to the principle of frequency response function estimation, the modal parameters of the model can be obtained based on the analysis of the power spectral density function of the acceleration response of the model.

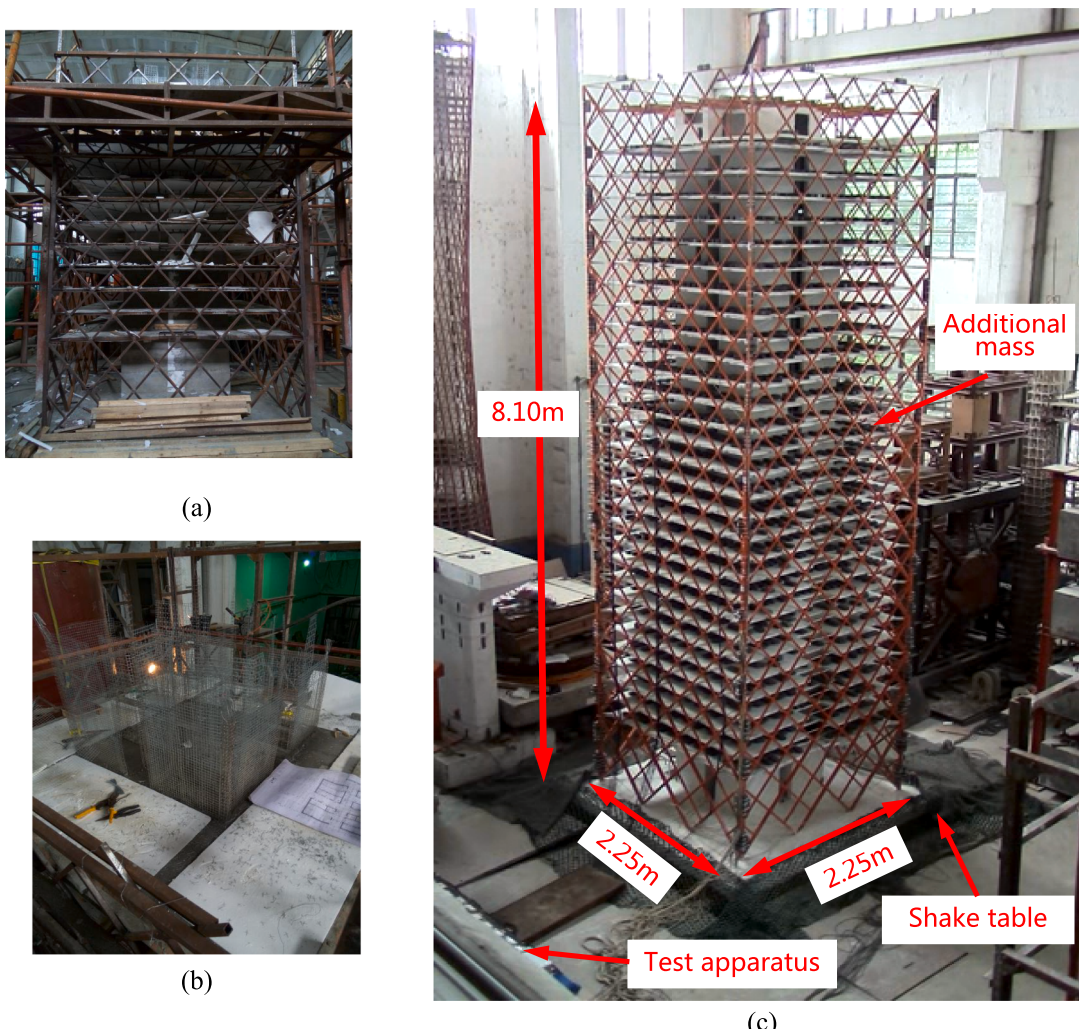


**Fig. 5.** (a) Construction of model diagrid frame; (b) assembling the formwork for RC structural wall and the slab; (c) test model setup on the shaking table.

**Table 8**

Numbering of accelerometer (Ach) and displacement meter (Dch) for test model.

No.	Location and direction				
	A1(slab) X-direction	B1(slab) Y-direction	C1(slab) in X- and Y-direction	D1(Perimeter diagrid) X-direction	E1(Perimeter diagrid) Y-direction
Top	Dch10	Dch20	Ach28/36	Ach48	Ach55
33	Dch09	Dch19	Ach27/35	Ach62	Ach69
29	Dch08	Dch18	Ach26/34	Ach47	Ach54
25	Dch07	Dch17	Ach39/40	Ach61	Ach68
21	Dch06	Dch76	Ach25/33	Ach46	Ach53
17	Dch05	Dch75	Ach24/32	Ach45	Ach52
13	Dch74	Dch14	Ach23/31	Ach44	Ach51
9	Dch73	Dch13	Ach22/30	Ach43	Ach50
5	Dch72	Dch12	Ach77/29	Ach42	Ach49
1	Dch71	Dch57	Ach37/38		

#### 2.4. Ground motion selection and scaling

The seismic shaking intensity VII on the site condition II has been considered for the building based on the 2010 CCSDB (NSPRC 2010a). One set of artificial ground motion (AGM) designated by the local seismological bureau and three sets of recorded ground motions (El Centro, Chichi, and Loma Prieta records) have been selected in this study based on the site soil classification (Class II) in the detailed geotechnical investigation. The shake table was excited in a unidirectional loading mode, with unidirectional input ground vibrations in the X and Y directions of the building structure model, respectively. Fig. 6 shows the response spectra of the AGM, El Centro, Chichi, and Loma Prieta records in X direction and the average response spectrum of the service level

earthquake (SLE), the design-based earthquake (DBE), and the maximum credible earthquake (MCE). The ground motions have been amplitude scale, where the scaled PGAs are 0.17 g, 0.49 g, and 0.88 g in the shaking table tests, for the SLE, DBE, and MCE, respectively.

The ground motions have been applied in the sequence of AGM, El Centro, Chichi, followed by Loma Prieta records (Fig. 7). As the ground motions are shown in Fig. 7, the 1/20 scale model has been tested by the shake table test under the AGM, El Centro, Chichi, followed by Loma Prieta seismic records.

### 3. Experimental responses and observation

#### 3.1. Global response

The input PGA was evaluated after completion of each test loading condition to satisfy the error control of obtaining the peak acceleration of the first story and the design PGA within 5%. Development and width of cracks were marked and measured using steel ruler for all stories. Table 9 shows the loading PGAs and the achieved maximum accelerations of the test model in 1st story, 17th story, and 36th story, respectively. From Table 9 it is illustrated that the maximum acceleration responses of the test model increased by 75%~200% at the top story under the different service levels of the seismic excitations.

The displacement responses of the bottom and top stories near the core tube, the maximum drifts occur in the top story, and total building drifts are similar in X- and Y-direction under different ground motions, which indicate the structural stiffnesses are the same in the two directions. Fig. 8 present the time-history displacements in the top story along the X-direction for the test model subjected to the ground motions under the MCE hazard level. The maximum roof drift is approximately

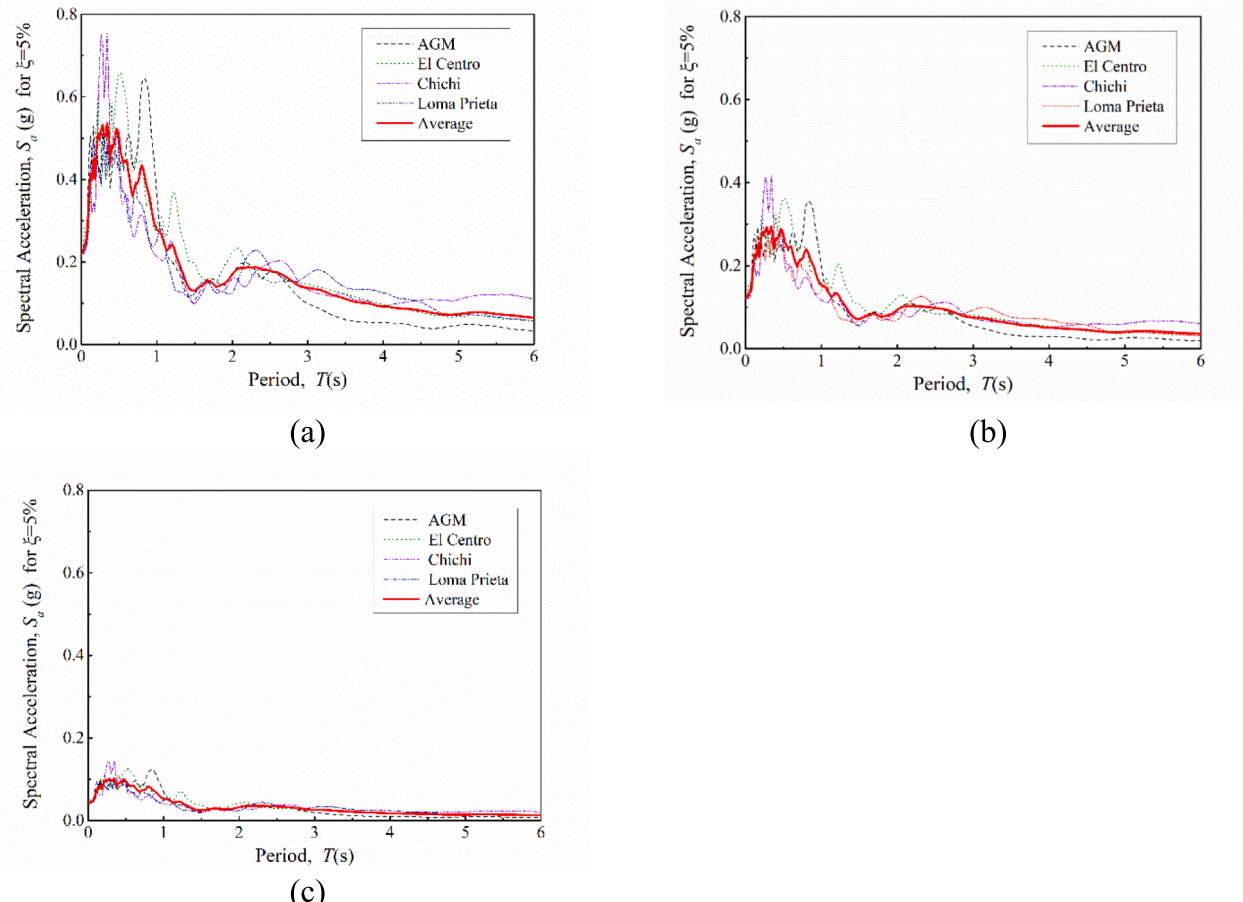
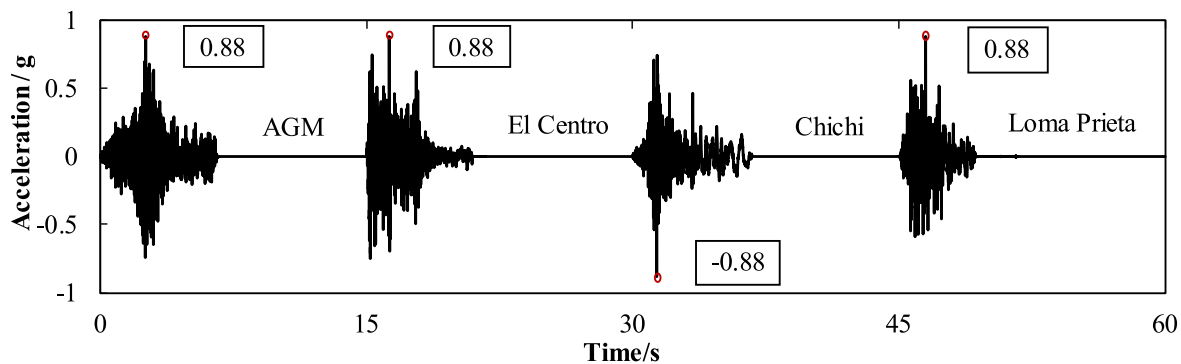


Fig. 6. Response spectra of SLE (a), DBE (b), and MCE (c) levels.



**Fig. 7.** Acceleration time history of ground motions at MCE level.

**Table 9**  
Loading cases of ground motions and response of model.

Service level	No.	Seismic wave	Design PGA (g)	Achieved maximum acceleration (g)		
				Story 1	Story 17	Story 36
SLE	1	White noise	0.05	0.05	–	–
	2	AGM	0.17	0.16	0.25	0.44
	3	El Centro 1940	0.17	0.17	0.25	0.49
	4	Chi-Chi 1999	0.17	0.16	0.18	0.41
	6	Loma Prieta 1989	0.17	0.16	0.18	0.34
	6	White noise	0.05	0.05	–	–
DBE	7	AGM	0.49	0.48	0.85	1.41
	8	El Centro 1940	0.49	0.47	0.80	1.37
	9	Chi-Chi 1999	0.49	0.42	0.68	1.14
	10	Loma Prieta 1989	0.49	0.47	0.66	0.96
	11	White noise	0.05	0.05	–	–
	12	AGM	0.88	0.89	1.36	2.24
MCE	13	El Centro 1940	0.88	0.88	1.34	2.22
	14	Chi-Chi 1999	0.88	0.89	0.95	1.56
	15	Loma Prieta 1989	0.88	0.84	0.96	1.66
	16	White noise	0.05	0.05	–	–

27.71 mm when the model subjected to the Chichi ground motion scaled to the MCE level.

By using the Newton's first law, the base shear of the whole model can be determined based on the experimentally measured accelerations relative to the shake table and the corresponding mass of each story. Fig. 9 shows the roof drifts versus the base shear of the model subjected to AGM, El Centro, Chichi, Loma Prieta earthquakes under the MCE seismic hazard levels. The hysteresis curves of the integral model shown that the peak base shear and the top displacement do not occur simultaneously. This phenomenon is expected because the time delay amplification of displacement time history at the top of the high-rise structure compared with external seismic excitation at the bottom.

### 3.2. Strain distributions of bottom diagrid

As shown in Fig. 10a, the axial forces of the perimeter diagrid in the 1st story are studied by the strain gauges attached to the diagonal bracings (S1, S2, and S3). This strain of the steel diagonal bracing is presented herein because the horizontal seismic force from the shake table is converted into the axial force of the perimeter diagrid. Fig. 10b, c, and d represent the peak strain of the diagonal bracings at the bottom layer for the model subjected to the various earthquakes of SLE, DBE, and MCE, respectively. After the loading cases of ground motions, the

residual strain of each strain gauge is restored to 0, which indicates that the perimeter diagrid in the 1st story are in elastic state. It can be seen from Fig. 10b-d that the maximum strains of the diagonal bracings S1, S2 and S3 during DBE shaking are 195–293%, 207–315% and 244–310% of those during the SLE, respectively. Their maximum strains during MCE shaking are 125–174%, 121–171% and 122–189% of those during the SLE, respectively. Thus, the axial forces of the diagonal bracings increase gradually with the increase of the seismic loads in the 1st story.

The comparison of the peak strains of diagonal bracings S1, S2, and S3 at the different seismic hazard levels have been plotted in Fig. 11. Based on the comparison of strains, it can be seen that the perimeter diagonal bracings have not entered the yield state, which meets the requirement of the performance level 3 in the specification for concrete structures of the tall building [26], i.e., only minor damage occurs to the macrostructure and critical member elements. The test results show that differences of the strains exist in the different positions of the diagonal bracings in the same floor. The average maximum strains of the diagonal bracings S1 and S3 are as 357–363% and 258–275% times as that of diagonal bracing S2 at the three levels of ground motions, respectively. Since the horizontal seismic force is mainly transmitted from the diagonal and box beams to the diagrid system through the joints, the joints along the axial direction of the diagonal bracings have the important impact on their axial forces, as shown in Fig. 10a.

### 3.3. Failure modes

The ground motion simulation test of the shaker was conducted for two days. After the SLE shaking series, no obvious cracks have been found in the RC structural wall, and the perimeter diagonal bracings are undamaged. The modal parameter analysis of Gaussian white noise excitation showed that the characteristic frequencies of the model structure remained the same before and after the test. The results of the structural dynamic characteristics tests indicate that the model structure remains in an elastic state after the SLE series shaking action.

After DBE shaking, however, small horizontal cracks appeared in the structural walls between the 25th – 30th stories (Fig. 12a-b). Additionally, less additional deformation occurs in the perimeter diagonal bracing of the 25th – 30th stories. Gaussian white noise tests after the SLE series shaking showed that the characteristic frequencies of the model structure decreased due to cracks in the concrete structural walls.

After the MCE shaking series, the seismic damages of the model are further aggregated, where the previous cracks' width has increased (Fig. 12c-d). The beam-RC core joint and the beam-perimeter diagrid joint keep basically intact after the tests. Since the unbalanced horizontal force and the flexural moment between the RC core and the perimeter diagrid system are transferred through the diagonal beam, the plastic deformations begin to appear near the end of the diagonal beams (Fig. 12e). Meanwhile, severe damages of the concrete slabs have occurred due to the deformation of the beams (Fig. 12f). For the perimeter diagrid system, the plastic buckling mostly appears in the

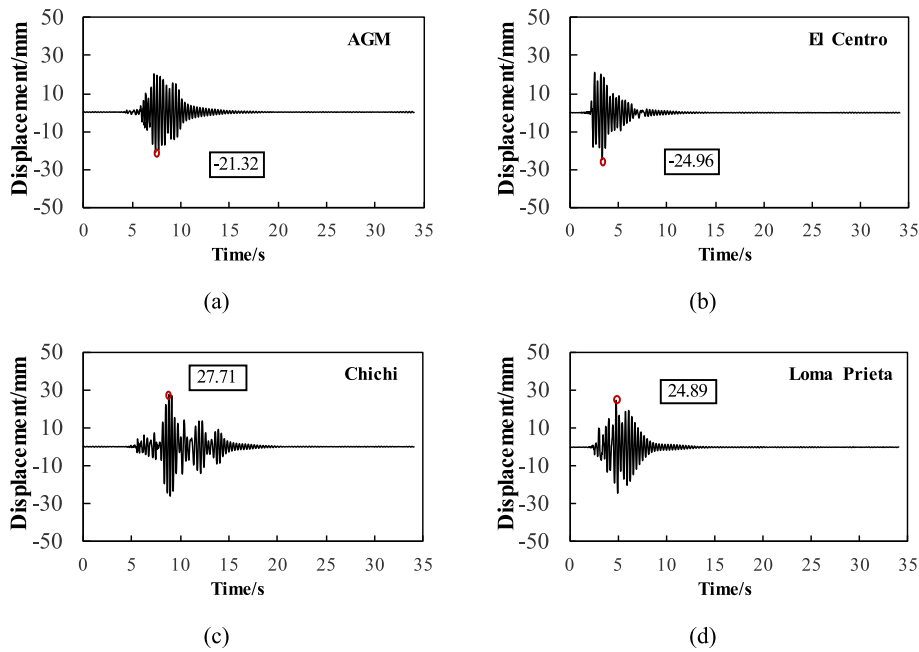


**Fig. 8.** Roof drifts in the X-direction under MCE seismic hazard level: (a) AGM, (b) El Centro, (c) Chichi, and (d) Loma Prieta.

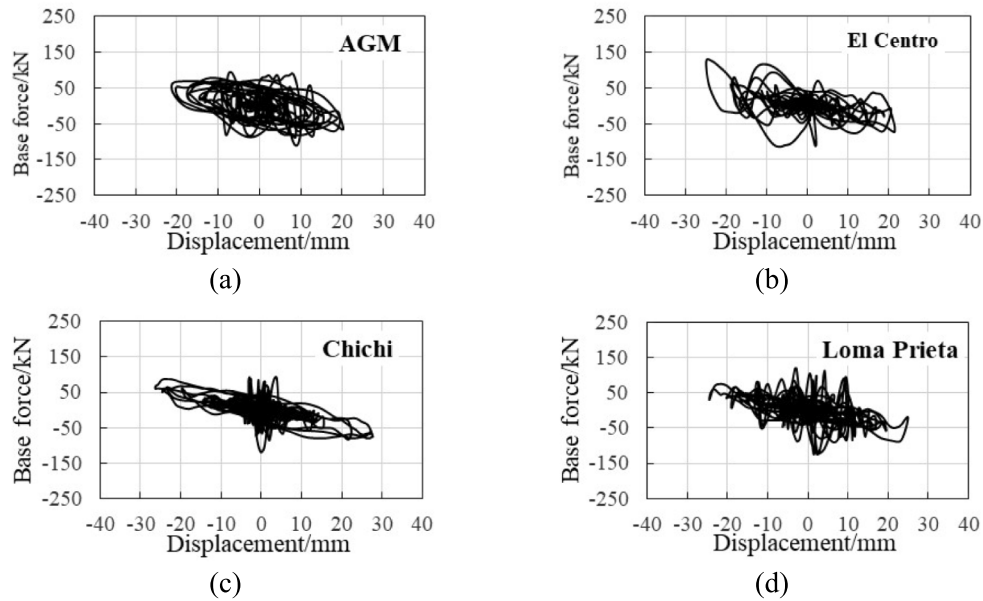


**Fig. 9.** Model roof drifts along the X-direction under MCE seismic hazard level: (a) AGM, (b) El Centro, (c) Chichi, and (d) Loma Prieta.

adjacent diagonal bracings in the 28th-30th stories (Fig. 12g-i), where the section size of the bracing is abruptly reduced in the adjacent stories. Nonetheless, the model structure still maintained a life safety condition without the onset of the partial or the total collapse after series of shaking table tests, which shows that the PDCC has robust seismic capacity against collapse under cycles of earthquake shaking.

#### 4. Comparison of finite element analysis and test

##### 4.1. Nonlinear finite element model

In order to verify results of the experimental tests of the PDCC structure under different seismic hazard levels, a series of nonlinear time history analyses were performed using the FEM of the prototype

structure. The prototype PDCC building was analyzed using the state-of-the-art FEM software, OpenSees (add reference). The diagrid structure has been modeled using the displacement-based nonlinear fiber beam-column model. The material properties (compressive and tensile strength) have been designed according to the 2010 Chinese concrete structure design code (CCSDC) [25]. The RC core wall is modeled using the beam-column element with a fiber discretized section which has been utilized in the response of the composite structural walls by Olabi et al. [27]. As for the confined and unconfined concrete constitutive relationship in CCSDC [25], the modified Kent and Park model [28] have been employed in this simulation. Thus, both the confined and the unconfined concrete property have been simulated using the *Concrete02* model [29,30], while the steel reinforcement has been used the *Steel02* model in OpenSees [31].

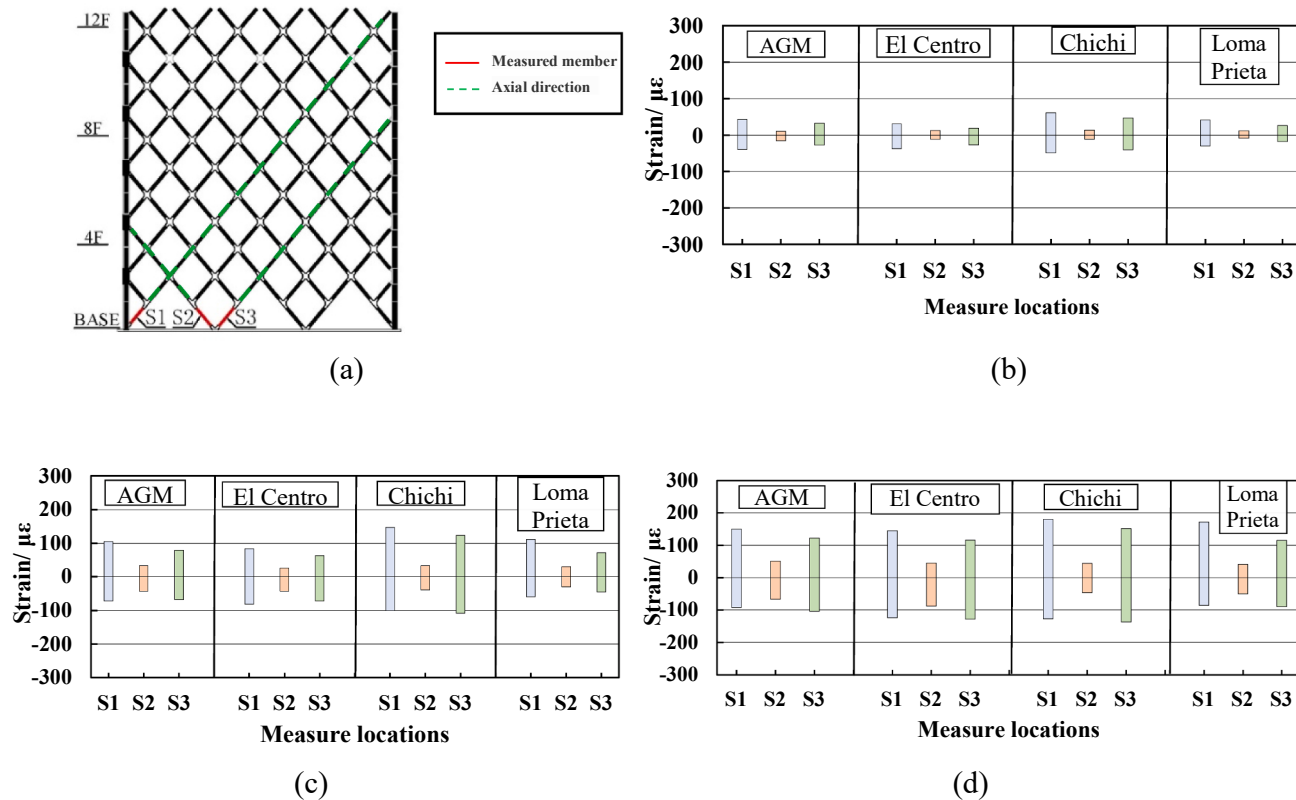


**Fig. 10.** Layout of strain gauges attached to bottom diagrid (a) and peak strains of model subjected to ground motions of SLE (b), DBE (c), and MCE (d).

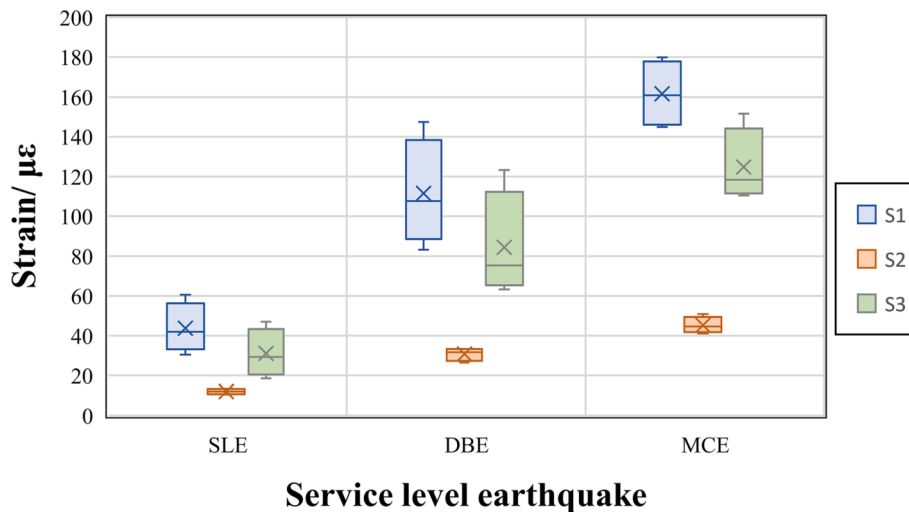


**Fig. 11.** Comparison of peak strains of diagonal bracings during SLE, DBE, and MCE.

The typical diagonal bracing uses steel with a yield strength of 345 MPa, and the stress-strain relationship for the monotonic envelope of the steel in tension is shown in Fig. 13(a). The stress-strain relationship for the monotonic envelope of concrete material (cubic compressive strength of 60 MPa) in compression is shown in Fig. 13(b). The effects of bond-slip behavior are neglected in this study. To solve the convergence problem of the analysis computation under large deformation, the norm of the iterative displacement increment developed in OpenSees has been utilized in the numerical analysis.

To verify the accuracy of the proposed model, the approach has been implemented to simulate the cyclic response of an RC structural wall tested by Lu et al. [32]. The confined concrete, the unconfined concrete,

and the steel reinforcement in the structural wall section are discretized with the fiber element in different sizes, as shown in Fig. 14. The material strength, the elastic modulus, and the stress-strain relationship of the concrete and the steel reinforcements are determined by the uniaxial mechanical property test. The material characteristic parameters and the geometric dimensions of the RC structural wall have been selected directly from Structural Wall Database [32]. The finite element simulation of the concrete structural wall is established by using the aforementioned material constitutive relation of the concrete and steel reinforcement. The typical structural wall is divided into five nonlinear fiber beam-column elements along the length direction. Fig. 15 shows the comparison of the hysteresis loop from the numerical simulation and

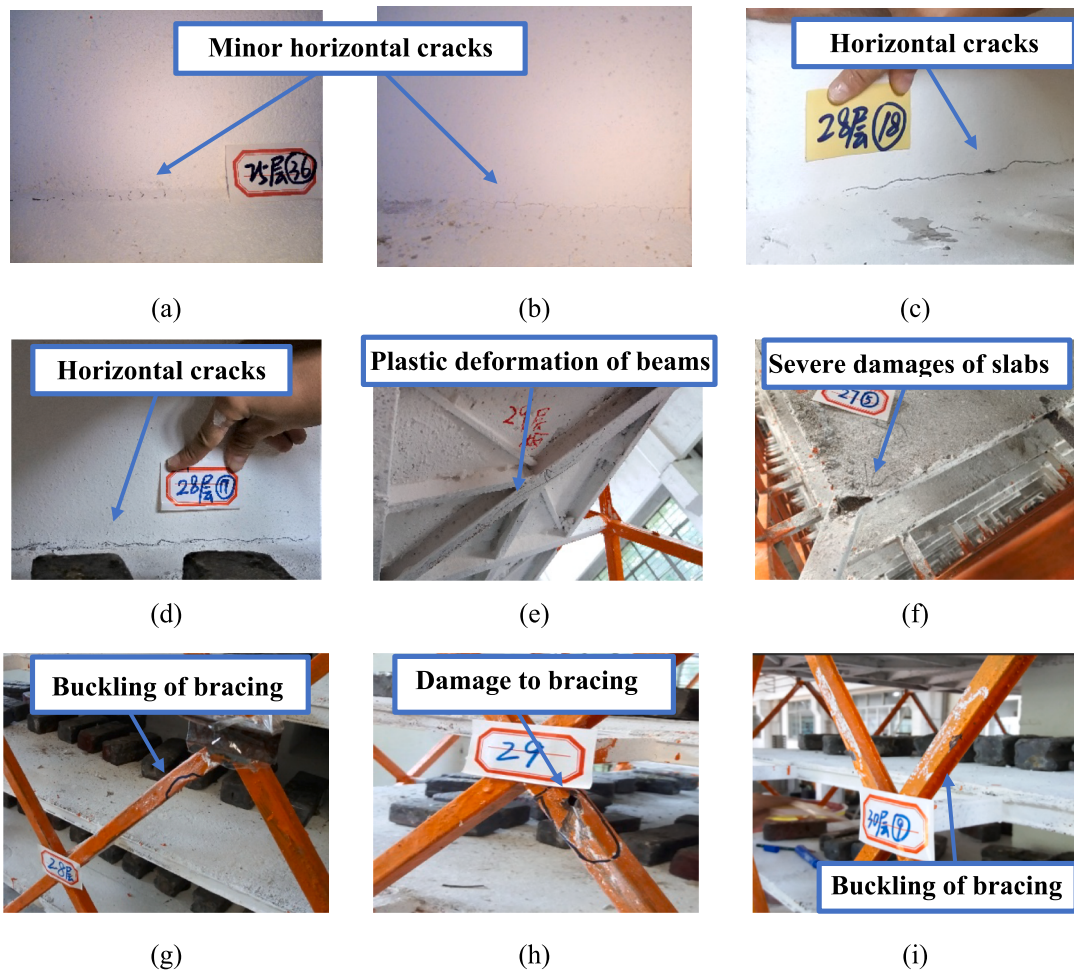


**Fig. 12.** Damages and failures of model structure in shaking table tests: (a) fine cracks of structural wall in 25th story; (b) fine cracks of structural wall in 28th story; (c) moderate cracks of structural wall in 28th story; (d) deformation of beam in 29th story; (f) severe damage of concrete slab in 27th story; (g) moderate buckling of diagonal bracings in 28th story; (h) serious buckling of diagonal bracings in 28th story; (i) slight buckling of diagonal bracings in 30th story.

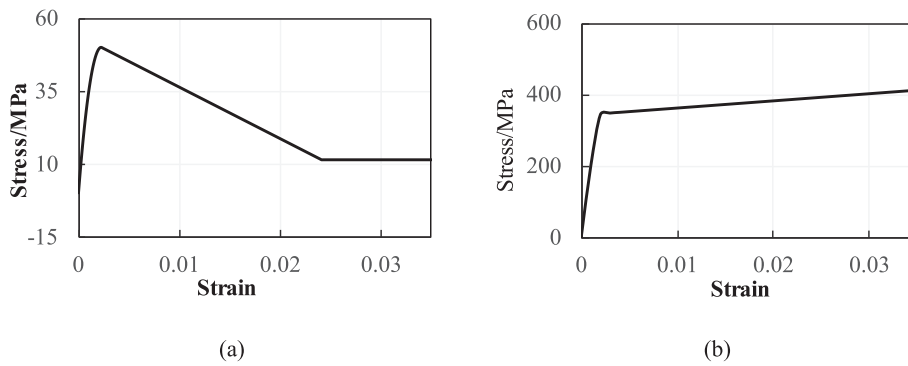


**Fig. 13.** Stress-strain relationships for monotonic envelopes of materials.

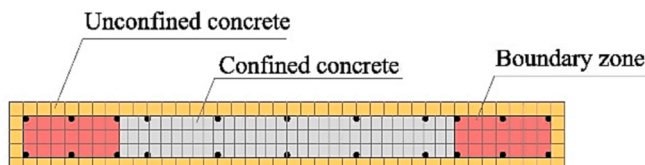


**Fig. 14.** Finite element meshes of structural wall.

experimental testing. The result shows the modeling approach can effectively simulate the nonlinear response of the RC wall. Since the FEM simulations mainly pay attention to the verification of the seismic behavior of the reduced scale model. Thus, the bond-slip and some other factors, such as the beam-to-column and beam-to-wall connections, will be discussed via further study.

As shown in the above experimental phenomena, the buckling effect is the important factor that contributes to the failure of the diagonal steel bracings. For the buckling prediction of the space steel structure, many effective constitutive models have been deduced and verified through

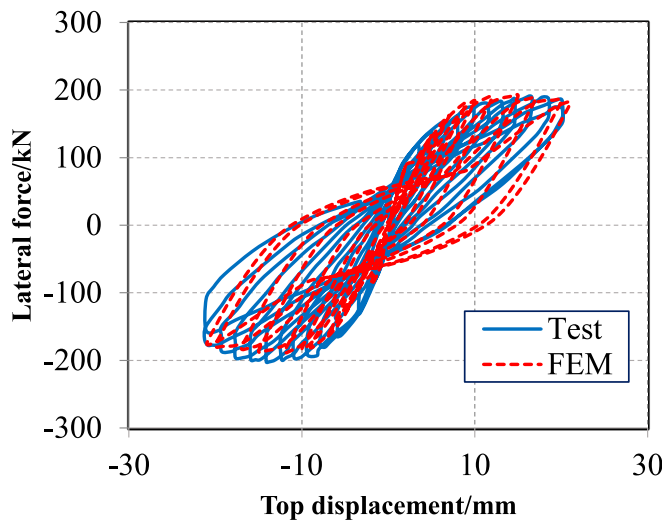


**Fig. 15.** Comparison of simulated and measured hysteretic curve [32].

the nonlinear dynamic analysis [33,34,35,36,37,38]. To simulate the inelastic buckling behavior of the perimeter steel diagrid, the force-based model for the large displacement has been used for the inelastic beam-column element in the OpenSees, which has been verified by the inelastic analysis of the cyclic buckling with different cross-sections [39]. Newmark time integration method incorporating a Rayleigh damping is used to solve the equation of motion.

Fig. 16 shows the 3D finite element model of the prototype PDCC

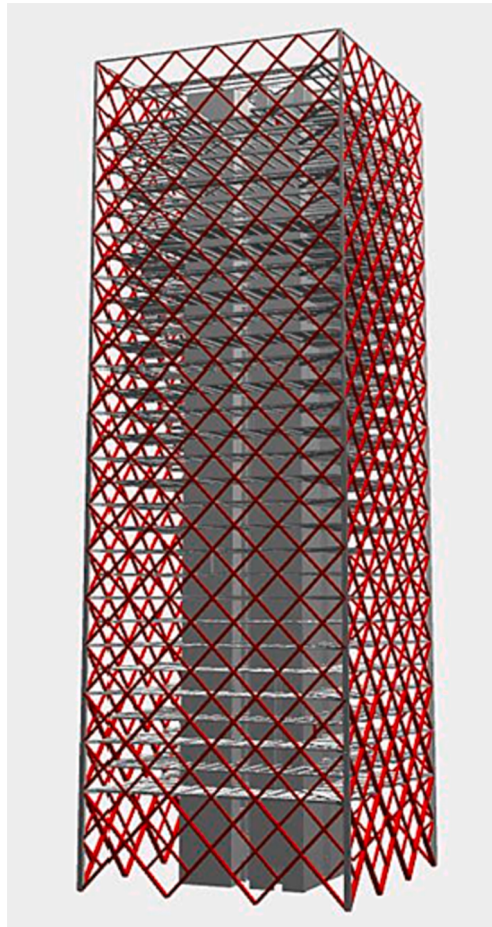


**Fig. 16.** Finite element model of PDCC structure.

building developed in OpenSees. The P-delta effect has been modeled using the P-delta geometry nonlinearity in OpenSees. The mass has been assigned to the model using the lumped mass according to the tributary area. The Newmark method is used to numerically integrate the dynamic response time steps of the structure. The convergence criteria are tested using the Norm Displacement Increment Test Method [13]. The 3.5% Rayleigh damping specified in the code (NSPRC 2010a) is used to assign to the main vibration modes in the finite element analysis of the structure according to the design company's requirements. The foundation is assumed to be rigid at the ground level, and the soil-structural interaction is not modeled.

In the finite element simulation, the seismic excitations used in the experiments have been scaled to the prototype according to the scale coefficient in Table 5. The results show that the equivalent fundamental frequencies scaled to the prototype structure are 0.41 Hz, 0.41 Hz, and 1.35 Hz for the first, second, and third vibration models according to the experimental measurement, respectively. These measured results are close to the numerical simulation results shown in Table 10. The corresponding three modes of vibration have been shown in Fig. 17.

#### 4.2. Comparison of finite element analysis and test results

The damage mechanism of the PDCC structure was analyzed based on the results of the experimental tests and numerical simulations. The maximum interstory drift of the experiment and numerical simulation, under the level action of SLE, was 1/1050 and 1/1100, respectively. The test observations showed that no significant cracks were found in the concrete structure walls and no damage was found in the perimeter diagonal system. The natural frequencies of the 1st, 2nd and 3rd modes of this phase all decreased by 1% from the initial state. Therefore, the test and simulation results indicate that the PDCC structure is in the elastic phase under the level action of SLE, and the concrete structure wall and the perimeter diagonal system co-resist the horizontal seismic action.

The maximum interstory drift of the experiment and numerical simulation, under the action of DBE level, was 1/397 and 1/402, respectively. After the test, small horizontal cracks of less than 1 mm were found at the 25th and 28th stories, respectively, and no damage was observed in the external diagonal bracing. The results of finite element calculations showed that the maximum tensile stress in the external diagonal braces at the 28th-30th floors reached 362 MPa, which exceeded the yield strength of the reinforcement (345 MPa). The natural frequencies of the 1st, 2nd and 3rd modes at this stage decreased by 5%, 5% and 4%, respectively, from the initial state. The overall model structure is closer to the elastic-plastic state.

The maximum interstory drift of the model under the effect of MCE levels is shown in Fig. 18. For the AGM, El Centro, Chichi and Loma Prieta earthquakes, the maximum interlayer drifts of the model were 1/257, 1/239, 1/217 and 1/234 in the experimental test, respectively. The maximum inter-story drifts obtained from numerical simulations are 1/270, 1/238, 1/229, and 1/228, respectively. The maximum inter-story drift of both tests and simulations occurred at the 25th-30th stories. As shown in Fig. 12c-i, the test observation revealed 1–2 mm horizontal cracks in the concrete structural wall around the 28th floor. The diagonal beam at the 27th floor was damaged at its connection with the floor slab, and the diagonal beam at the 29th floor was plastically deformed. Several external diagonal braces on the 29th floor showed buckling

**Table 10**  
Comparison of measured and simulated natural frequencies.

Mode	Equivalent prototype from experiment (Hz)	Numerical simulation (Hz)	Error (%)
1 ( $X$ translation)	0.41	0.44	6.8
2 ( $Y$ translation)	0.41	0.44	6.8
3 (Torsion)	1.35	1.30	3.8

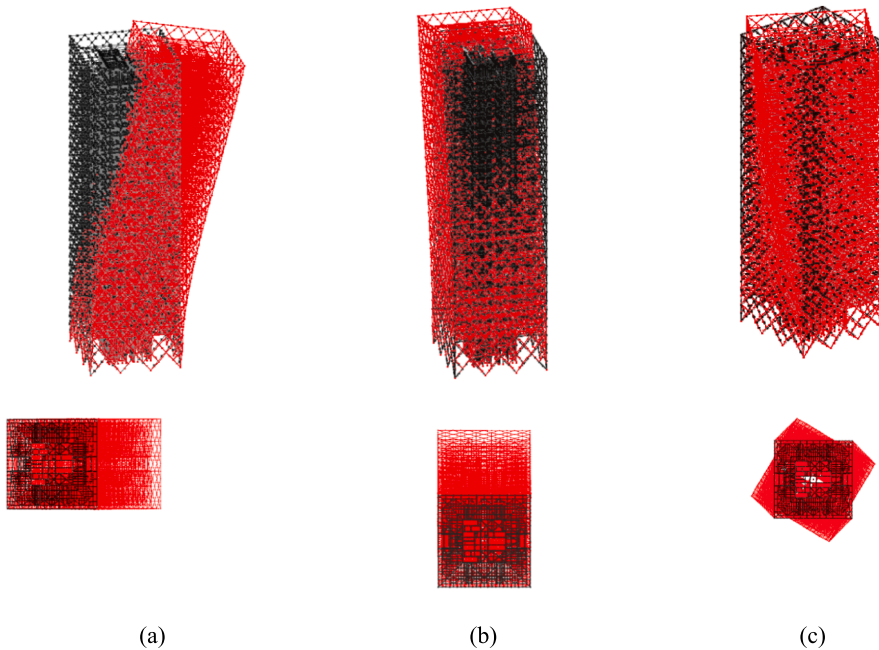


**Fig. 17.** Mode of vibration: (a) 1st mode, (b) 2nd mode and (c) 3rd mode.

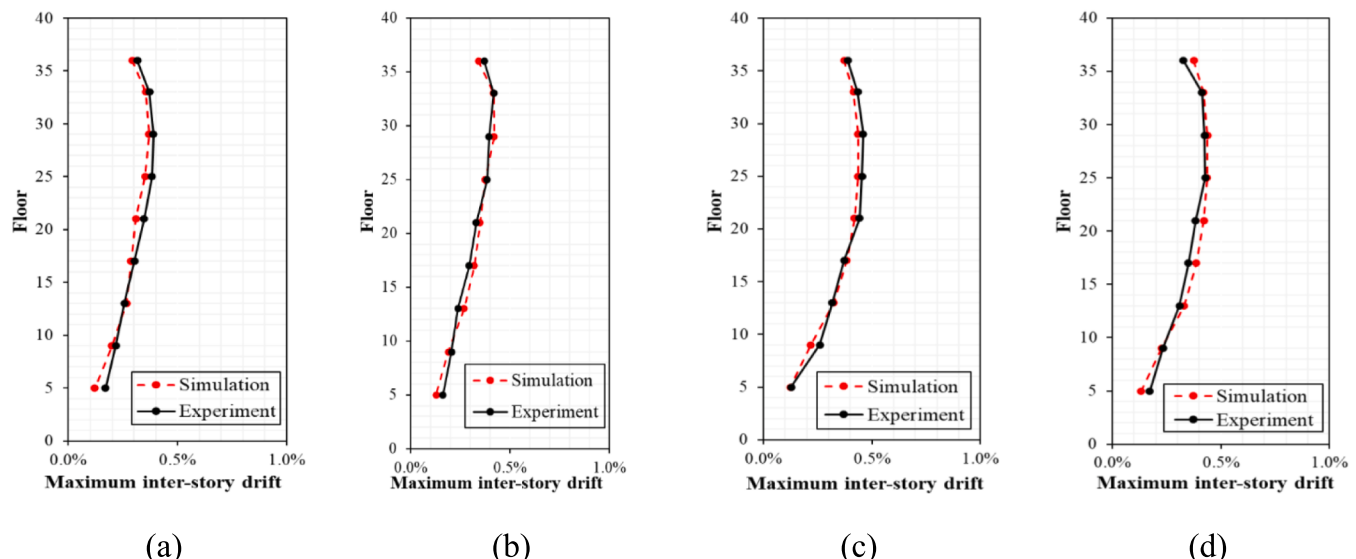


**Fig. 18.** Comparison of experimental versus simulated maximum inter-story drifts under MCE seismic hazard level: (a) AGM, (b) El Centro, (c) Chichi, (d) Loma Prieta.

damage, concentrated in the diagonal brace axial force higher members (more members were connected in the axial force direction). At the same time, buckling damage was also observed in the diagonal braces of the 28th and 30th floors. The numerical simulation results show that the stresses of several external diagonal cross-net diagonal braces in the middle of the 28th and 29th floors reach the steel yield strength of 470 MPa. When the stress of the diagonal brace reaches the yield strength, the diagonal brace is damaged at the same time, the damage has a tendency to expand to the surrounding diagonal brace. After the MCE horizontal earthquake, the natural frequencies of the 1st, 2nd and 3rd modes decreased by 12%, 12% and 8%, respectively, compared with the initial state. The above experimental and numerical analysis results indicate that the overall structure enters the elastic-plastic phase.

## 5. Summary and conclusions

Owing to the restriction of the test equipment, the high-rise building is difficult to be tested by the shaking table with large-scale model. Shaking table tests of 1/20 scale model have been carried out due to the lack of the comprehensive understanding of the seismic performance of the high-rise PDCC structure. Although to simulate the actual seismic behaviour of a concrete core tube structure with a small-scaled model is confronted with many problems such as the gravity distortion and the simulation of the nonlinearity of the concrete materials, the combination of experiment and nonlinear finite element numerical simulation helps to understand the seismic failure mode and the seismic performance of the newly developed PDCC structure system. The earthquake damage and the failure mode of the whole building under different seismic hazard levels have been investigated based on the observation of

the experiments and the FEM simulation studies. The conclusions are as follows:

1. The strains of the perimeter diagrid braces on the first floor have been monitored under different earthquake excitations, and the results show that the strains of the diagonal bracings in the same story are quite different, which confirms that the axial forces distribution in the perimeter diagrid bracings are uneven. And, the axial force of the external diagonal brace is related to the number of other diagonal braces on its axis. This is mainly because the floor beams transfer horizontal seismic forces and vertical loads to the diagonal bracing system through the nodes. The more other diagonal braces and nodes are connected in the direction of the diagonal brace axis, the more seismic forces and vertical loads will be transmitted by the floor beams.
2. The maximum inter-story drifts measured in the shaking table tests are basically consistent with the FEM simulations at the three levels of ground motions. The maximum inter-story drifts appear in the 25th-30th stories when subjected to ground motions at MCE level, where the section size of the bracing is abruptly reduced in the adjacent stories. The most severe seismic damage is concentrated in the diagonal braces with higher axial forces. While buckling and additional deformation also occurred in other adjacent diagonal braces, the damage was less severe in the diagonal brace with smaller axial force. More importantly, damage occurs when the diagonal bracing reaches yield strength, and the damage has a tendency to expand to the surrounding diagonal bracing.
3. According to the shape of the maximum inter-story drifts, the deformation response of structure is mainly presented with the bending deformation. The lateral displacement of PCDD structure is small and meets the requirement of performance level for concrete structures of tall building. The whole structure model still maintains

the life safety condition after all the shaking table tests. Both the experimental and numerical responses indicates that the floor slab system can effectively connect the perimeter diagonal system and the concrete core to form an efficient seismic force resisting system for high-rise building applications.

As for the dynamic analysis of the PDCC structure under the earthquakes, the seismic performance and the damage mechanism are affected not only by the stiffness of the floor and the joint, but also by the bond-slip between the longitudinal bars and surrounding concrete due to large deformations. These factors are hard to be considered in the shaking table test with the small-scaled model, which is necessary to carry out the theoretical and experimental research in the future.

#### CRediT authorship contribution statement

**Di Wu:** Conceptualization, Methodology, Data curation, Software. **T. Y. Yang:** Writing – original draft. **Yan Xiong:** Investigation, Software, Validation. **Solomon Tesfamariam:** Writing – review & editing.

#### Declaration of Competing Interest

The authors declare that they have no known competing financial interests or personal relationships that could have appeared to influence the work reported in this paper.

#### Acknowledgements

The authors are thankful for the support from Science and Technology Planning Project of Guangdong Province (2018B02028003), National Natural Science Foundation of China (52178281, 51778160), Science and Technology Program of Guangzhou (201831826).

## Appendix

Assuming that 3 primary variables are considered, the independent primary variables can be represented by the basic dimensional units as.

$$\begin{aligned} l &= L \\ a &= LT^{-2} \\ e &= FL^{-2} \end{aligned} \tag{A1}$$

Thus, the independent solution of the basic dimensional unit is.

$$\begin{aligned} L &\doteq l \\ T &\doteq (l/a)^{0.5} \\ F &\doteq el^2 \end{aligned} \tag{A2}$$

From this, substituting the above basic units for the other variables gives.

$$\begin{aligned} t &= T \doteq (l/a)^{0.5} \\ \rho &= FT^2 / L^4 \doteq e / (la) \\ m &= FT^2 / L \doteq el^2 / a \\ q &= F \doteq el^2 \\ f &= 1/T \doteq (a/l)^{0.5} \\ \epsilon &= 1 \\ \sigma &= F/L^2 \doteq e \\ \delta &= L \doteq l \end{aligned} \tag{A3}$$

When the geometric similarity ratio is small, the materials in the reinforced concrete members of the model structure are in a low stress state, which makes it difficult to achieve similar relationships for the strength of the member sections. In order to achieve similarity in the load-bearing capacity of the concrete members, longitudinal reinforcement and the stirrup of the model structure is designed by using the bending moment and shear force equivalence of the concrete members [20]. The bending moment and shearing force of the concrete members of the prototype and model structure can be expressed as.

$$\begin{aligned} B^p &= f_y^p A_s^p h_0^p, V^p = \frac{f_{yv}^p A_{sv}^p h_0^p}{s^p} \\ B^m &= f_y^m A_s^m h_0^m, V^m = \frac{f_{yv}^m A_{sv}^m h_0^m}{s^m} \end{aligned} \quad (\text{A4})$$

where  $B^p$ ,  $V^p$ ,  $B^m$ , and  $V^m$  are the bending moment and the shear force of the prototype and the model structure, respectively.  $A_s^p$ ,  $A_{sv}^p$ ,  $A_s^m$ , and  $A_{sv}^m$  are the sectional area of the longitudinal reinforcement and the stirrup for the prototype and the model, respectively.  $s^p$  and  $s^m$  are the scale factor for the spacing of stirrups of the prototype and model structure, respectively.  $S_{f_y}$  and  $S_{f_{yv}}$  refer to the scale factor for the tensile strength of the longitudinal reinforcement and the stirrup, respectively.  $h_0^p$  and  $h_0^m$  are the effective depth of section of the prototype and model, respectively.

According to Eq. (A.4), the scale factor for bending moment ( $S_B$ ) and shear force ( $S_V$ ) of the member can be obtained as.

$$\begin{aligned} S_B &= \frac{A_s^m}{A_s^p} S_L \cdot S_{f_y} \\ S_V &= \frac{A_{sv}^m}{A_{sv}^p} S_{f_{yv}} \cdot \frac{S_L}{S_s} \end{aligned} \quad (\text{A5})$$

where  $S_l$  is the geometric scale factor,  $S_s$  is the scale factor for the spacing of stirrups,  $S_{f_y}$  and  $S_{f_{yv}}$  refer to the scale factor for the tensile strength of the longitudinal reinforcement and the stirrup, respectively.

## References

- [1] K. Moon, Design and construction of steel diagrid structures, 11th Nordic Steel Construction Conference (NSCC 2009), Swedish Institute of Steel Construction, Uppsala, Sweden, 2009, pp. 398–405.
- [2] G.M. Montuori, E. Mele, G. Brandonisio, A. De Luca, Secondary bracing systems for diagrid structures in tall buildings, *Eng. Struct.* 75 (2014) 477–488.
- [3] X. Lu, H. Jiang, Recent progress of seismic research on tall buildings in China mainland, *Earthq. Eng. Eng. Vib.* 13 (S1) (2014) 47–61.
- [4] W.H. Chen, Z.R. Lu, W. Lin, S.H. Chen, Y.Q. Ni, Y. Xia, W.Y. Liao, Theoretical and experimental modal analysis of the guangzhou new TV tower, *Eng. Struct.* 33 (12) (2011) 3628–3646.
- [5] A. Fakhraddini, S. Hamed, M.J. Fadaee, Peak displacement patterns for the performance-based seismic design of steel eccentrically braced frames, *Earthq. Eng. Eng. Vib.* 18 (2) (2019) 379–393.
- [6] T. Li, T.Y. Yang, G. Tong, D.P. Tung, Y. Li, Performance-based seismic design and evaluation of fused steel diagrid frame, *Earthq. Spectra.* 34 (4) (2018) 1869–1891.
- [7] R.J. Liptack, Motion based seismic design and loss estimation of diagrid structures, Massachusetts Institute of Technology (2013).
- [8] C. Liu, K. Ma, X. Wei, G. He, W. Shi, Y. Zhou, Shaking table test and time-history analysis of high-rise diagrid tube structure, *Period. Politecno-Civ. Eng.* (2016), <https://doi.org/10.3311/PPci.9243>.
- [9] J. Lee, J. Kong, J. Kim, Seismic performance evaluation of Steel Diagrid Buildings, *Int. J. Steel Struct.* 18 (3) (2018) 1035–1047.
- [10] K. Kamath, S. Hirannaiah, J.C.K.B. Noronha, An analytical study on performance of a diagrid structure using nonlinear static pushover analysis, *Perspect. Sci.* 8 (2016) 90–92.
- [11] E. Asadi, Y. Li, Y. Heo, Seismic performance assessment and loss estimation of steel diagrid structures, *J. Struct. Eng.* 144 (10) (2018) 04018179.
- [12] J. Kim, Y.-H. Lee, Seismic performance evaluation of diagrid system buildings, *Struct. Des. Tall Spec. Build.* 21 (10) (2012) 736–749.
- [13] S. Mazzoni, F. McKenna, M.H. Scott, et al., OpenSees command language manual, *Pacific Earthq. Eng. Res. Cent.*, 2006.
- [14] National Standard of the People's Republic of China (NSPRC). Load Code for the Design of Building Structures (GB50009-2012), China Architecture & Building Press, Beijing, China, 2012.
- [15] National Standard of the People's Republic of China (NSPRC). Chinese Code for Seismic Design of Buildings (GB50011-2010), Ministry of Construction of Peoples Republic of China, Beijing, China, 2010a.
- [16] National Standard of the People's Republic of China (NSPRC). Chinese Code for Design of Steel Structures (GB50017-2003), Ministry of Construction of Peoples Republic of China, Beijing, China, 2003.
- [17] H.G. Harris, G.M. Sabin, *Structural modeling and experimental techniques*, CRC Press, New York, 1999.
- [18] K. Yuan, D. Gan, J. Guo, et al., Hybrid geotechnical and structural seismic isolation: Shake table tests, *Earthq. Eng. Struct. Dyn.* 50 (12) (2021) 3184–3200.
- [19] A.J. Rosakis, J.E. Andrade, V. Gabuchian, et al., Implications of Buckingham's Pi theorem to the study of similitude in discrete structures: Introduction of the RFN, *μN*, and SN dimensionless numbers and the concept of structural speed, *J. Appl. Mech.* 88 (9) (2021), 091008.
- [20] X. Lu, Y. Zhou, W. Lu, Shaking table model test and numerical analysis of a complex high-rise building, *Struct. Des. Tall Spec. Build.* 16 (2) (2007) 131–164.
- [21] L.H. Han, W. Li, Y.F. Yang, Seismic behaviour of concrete-filled steel tubular frame to RC shear wall high-rise mixed structures, *J. Constr. Steel. Res.* 65 (5) (2009) 1249–1260.
- [22] C.S. Li, S.S. Lam, M.Z. Zhang, et al., Shaking table test of a 1:20 scale high-rise building with a transfer plate system, *J. Struct. Eng.* 132 (11) (2006) 1732–1744.
- [23] Y. Zhou, X. Lu, W. Lu, et al., Shake table testing of a multi-tower connected hybrid structure, *Earthq. Eng. Eng. Vib.* 8 (1) (2009) 47–59.
- [24] ACI Committee 318. Building Code Requirements for Structural Concrete (ACI 318-05) and Commentary (ACI 318R-05), American Concrete Institute, Farmington Hills, Mich, 2005.
- [25] National Standard of the People's Republic of China (NSPRC).Chinese Concrete Structure Design Code (GB50010-2010), Ministry of Construction of Peoples Republic of China, Beijing, China, 2010b.
- [26] Ministry of Housing and Urban-Rural Development (MHURD). Technical Specification for Concrete Structures of Tall Building (JGJ3-2010), Ministry of Housing and Urban-Rural Development of the People's Republic of China, Beijing, China, 2010.
- [27] M.N. Olabi, N. Caglar, M.H. Kisa, et al., Numerical study on the response of composite shear walls with steel sheets under cyclic loading, *J. Build. Eng.* 34 (2021), 102069.
- [28] D.C. Kent, R. Park, Inelastic behaviour of reinforced concrete members with cyclic loading, *Bull. N. Z. Soc. Earthq. Eng.* 4 (1) (1971) 108–125.
- [29] I.D. Karsan, J.O. Jirsa, Behavior of concrete under compressive loadings, *J. Struct. Div.* 95 (12) (1969) 2543–2564.
- [30] M.H.M. Yassin, *Nonlinear Analysis of Prestressed Concrete Structures under Monotonic and Cyclic Loads*, University of California, Berkeley, USA, 1994. PhD Thesis.
- [31] M. Menegotto, P.E. Pinto, Method of analysis for cyclically loaded reinforced concrete plane frames including changes in geometry and nonelastic behaviour of elements under combined normal force and bending, in: IABSE symposium on resistance and ultimate deformability of structures acted on by well defined repeated loads, Lisbon, 1973, pp. 15–22.
- [32] X.L. Lu, Y. Zhou, J.H. Yang, et al., Shear Wall Database, Dataset, Network for Earthquake Engineering Simulation (database), 2010.
- [33] C.D. Hill, G.E. Blandford, S.T. Wang, Post-buckling analysis of steel space trusses, *J. Struct. Eng.* 115 (4) (1989) 900–919.
- [34] B. Calderoni, A. De Martino, A. Formisano, et al., Cold formed steel beams under monotonic and cyclic loading: Experimental investigation, *J. Constr. Steel. Res.* 65 (1) (2009) 219–227.
- [35] G. Terracciano, G. Di Lorenzo, A. Formisano, et al., Cold-formed thin-walled steel structures as vertical addition and energetic retrofitting systems of existing masonry buildings, *Eur. J. Environ. Civ. Eng.* 19 (7) (2015) 850–866.
- [36] G. Di Lorenzo, A. Formisano, R. Landolfo, On the origin of I beams and quick analysis on the structural efficiency of hot-rolled steel members, *Open Civ. Eng. J.* 11 (1) (2017) 332–344.

- [37] F. Braga, R. Gigliotti, R. Laguardia, Intervention cost optimization of bracing systems with Multiperformance Criteria, *Eng. Struct.* 182 (2019) 185–197.
- [38] D. Wu, S. Tesfamariam, S.F. Stiemer, et al., Seismic fragility assessment of RC frame structure designed according to modern Chinese code for seismic design of buildings, *Earthq. Eng. Eng. Vib.* 11 (3) (2012) 331–342.
- [39] P. Uriz, F.C. Filippou, S.A. Mahin, Model for cyclic inelastic buckling of steel braces, *J. Struct. Eng.* 134 (4) (2008) 619–628.